





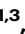


Declines in anthropogenic mercury emissions in the Global North and China offset by the Global South

Received: 12 August 2024

Accepted: 13 January 2025

Published online: 30 January 2025



Xinran Qiu ¹, Maodian Liu ^{1,2,3} ✉, Yuanzheng Zhang¹, Qianru Zhang ⁴, Huiming Lin¹, Xingrui Cai¹, Jin Li¹, Rong Dai¹, Shuxiu Zheng¹, Jinghang Wang¹, Yaqi Zhu¹, Huizhong Shen ^{5,6}, Guofeng Shen ^{1,3}, Xuejun Wang ^{1,3} ✉ & Shu Tao ^{1,3}

Human activities have emitted substantial mercury into the atmosphere, significantly impacting ecosystems and human health worldwide. Currently, consistent methodologies to evaluate long-term mercury emissions across countries and industries are scant, hindering efforts to prioritize emission controls. Here, we develop a high-spatiotemporal-resolution dataset to comprehensively analyze global anthropogenic mercury emission patterns. We show that global emissions increased 330% during 1960–2021, with declines in developed Global North countries since the 1990s and China since the 2010s completely offset by rapid growth in Global South countries (excluding China). Consequently, global emissions have continued to rise slightly since the 2013 Minamata Convention. In 2021, Global South countries produced two-thirds of global emissions, despite comprising only one-fifth of the global economy. We predict that, although large uncertainties exist, continued emission growth in Global South countries under a business-as-usual scenario could increase 10%–50% global mercury emissions by 2030. Our findings demonstrate that global control of anthropogenic mercury emissions has reached a critical juncture, highlighting the urgent need to target reductions in Global South countries to prevent worsening health and environmental impacts.

Human activities have increased global atmospheric mercury (Hg) levels by three to five times since industrialization^{1–3}. Mainly in the form of gaseous elemental Hg (Hg⁰), Hg⁰ can travel long distances, remains in the atmosphere for 6–24 months, and is eventually deposited on terrestrial and aquatic ecosystems^{4,5}. Once deposited, it can re-enter the atmosphere under certain conditions, exacerbating global Hg pollution^{6–8}. In waters and sediments, Hg can convert to the

neurotoxic methylmercury (MeHg)^{9,10}, which substantially accumulates in food webs^{11,12}, posing severe food safety and public health risks^{1,13,14}. To reduce Hg usage and emissions, the World Health Organization (WHO) listed Hg among the world's top ten chemicals of concern and the United Nations Environment Program (UNEP) proposed the Minamata Convention in 2013 with over 130 participating countries¹⁵.

¹Ministry of Education Laboratory of Earth Surface Processes, College of Urban and Environmental Sciences, Peking University, Beijing, China. ²School of the Environment, Yale University, New Haven, CT, USA. ³Institute of Carbon Neutrality, Peking University, Beijing, China. ⁴Nicholas School of the Environment, Duke University, Durham, NC, USA. ⁵Shenzhen Key Laboratory of Precision Measurement and Early Warning Technology for Urban Environmental Health Risks, School of Environmental Science and Engineering, Southern University of Science and Technology, Shenzhen, China. ⁶Guangdong Provincial Health Observation and Research Station for Coastal Atmosphere and Climate of the Greater Bay Area, Shenzhen, China. ✉e-mail: maodian.liu@pku.edu.cn; xjwang@urban.pku.edu.cn

Anthropogenic Hg emissions, primarily from fossil fuel combustion and industrial metal production, greatly determine global atmospheric Hg distribution and deposition^{16–18}. For centuries, developed Northern Hemisphere countries have predominately contributed to these emissions^{17,19}. Research indicated that atmospheric Hg concentrations have been higher in the Northern Hemisphere than in the Southern Hemisphere^{20–22}. However, since the 1990s, atmospheric Hg levels in Europe and North America have declined^{18,23,24}. China, the world's largest emitter, has also shown a recent downward trend^{25,26}, while trends in other Global South countries remain unknown^{21,27}. Despite the lack of long-term monitoring, limited observations suggest that atmospheric Hg concentrations are rapidly increasing in some Global South countries and in Antarctica since the 2010s^{19,28,29}. The Global South refers to less developed countries and regions in Africa, Latin America, Asia, and Oceania, typically contrasted with the Global North, which includes developed countries³⁰. It is urgent to determine whether the Global South, excluding China, now dominates global anthropogenic Hg emission trends. Answering this question is crucial for setting global priorities to reduce Hg emissions across different countries and sectors.

Atmospheric Hg concentrations reflect local emissions, regional transport, and meteorological influences¹⁶. To fully understand the source-sink relationships of global atmospheric Hg, compiling emission inventories and integrating them with process-based models and observations is essential^{5,18,31}. Although there are several inventory products for global and regional anthropogenic Hg emissions^{6,17,19,32–41}, most either focus only on specific years, lack detailed spatial distributions and emission sources, or do not include uncertainty analyses. Moreover, differences in modeling methods, activity levels, and emission factors among inventories create inconsistencies that prevent the straightforward merging of different inventories over time⁴¹. Therefore, using current inventories to provide a continuous and detailed temporal trend of global anthropogenic Hg emissions remains challenging. This also limits an accurate understanding of the spatial distribution patterns of global atmospheric Hg sources and sinks. Given that climate change could complicate the Hg cycle^{42–44}, this limitation hinders our ability to set Hg emission reduction targets compatible with specific climate change scenarios.

Here, we develop a long-term (1960–2021) dataset of global anthropogenic Hg emissions with high spatiotemporal resolution and fine sector classification. This dataset aims to determine whether emissions from the Global South, excluding China, have controlled the global emission trends, and to identify key countries and sectors for emission reductions. Compared to previous inventories of Hg, the new inventory offers several advantages: (1) consistent methods for estimating historical Hg emissions over the past 62 years, maximizing spatial ($0.1^\circ \times 0.1^\circ$) and temporal (annually from 1960 to 2021) resolutions and sector categorization (121 emission sources) of the inventory; (2) detailed investigations of Peking University Fuel Inventories (PKU-FUEL) on long-term fuel consumption, including point sources and extensive county/city/state data⁴⁵, with 16 types of biomass fuels detailed and Hg emissions from agricultural combustion sources are estimated for the first time^{19,46}; (3) updated Hg emission factors for most sectors to improve the accuracy of estimates; (4) use of Monte Carlo simulation to quantify historical uncertainty for each source in all countries. This robust foundation allows for assessing the effectiveness of the Minamata Convention and establishes a rational benchmark for global atmospheric Hg reduction.

Results and discussion

Rising global mercury emissions

Our analyses reveal that global anthropogenic Hg emissions to the atmosphere reached 2477 Mg in 2021 (–25% to 30%, interquartile range), a 3.3-fold increase from 1960 (Fig. 1a). Artisanal and small-scale gold mining (ASGM) and cement production are the primary drivers of

this increase, with ASGM emissions hitting 975 Mg (623–1327 Mg) in 2021, ten-fold greater than the level in 1960 (Fig. 1b). During this period, ASGM's share of total emissions increased by 26% (Fig. 1c), making it the largest emission source^{17,36,38,39,47}. Non-ferrous metal production, previously the largest anthropogenic Hg emission sector before the 1980s, has seen its global share continuously decline over the past 62 years (Fig. 1).

A pivotal shift in global anthropogenic Hg emissions occurred after 2013 with the signing of the Minamata Convention, marking a transition from rapid growth to stagnation. We divide the past 62 years of global missions into four stages (Fig. 1a) based on the trends of the emission curve: Stage I (1960–1980) was characterized by rapid growth driven by post-World War II economic expansion⁴⁸. Apart from non-ferrous metal production, the emissions began to grow in almost all sectors. Stage II (1980–2000) was a period of stable emissions due to the fluctuating gold price by international politics, leading to a decline in ASGM production and Hg emissions⁴⁹ (Fig. 1a). Moreover, increased attention to environmental pollution in Europe and the United States prompted the introduction of Air Pollution Control Devices (APCDs)⁵⁰, which partially offset emission increases from other countries.

Entering the 21st century, global anthropogenic Hg emissions have doubled. In stage III (2000–2013), the benefits of Hg phase-out in North America and Europe were largely realized³. Yet, the rapid expansion of emerging Asian economies led to a sharp increase in Hg emissions from sectors such as ASGM, fossil fuel combustion, and cement production (Fig. 1a). Stage IV (2013–present), following the Minamata Convention, increases in global Hg emissions from many sectors appear to be curbed, although most of them have not yet declined. Therefore, the Minamata Convention and related national emission reduction policies have temporarily halted the rapid rise in global anthropogenic Hg emissions, placing global control at a critical juncture.

Our estimates align with most previous studies^{6,17,19,32,33,36,38,39} (Supplementary Fig. 1). For instance, our 2015 estimate of 2316 Mg is slightly higher than the 2220 Mg reported by the Global Mercury Assessment 2018 (GMA 2018)¹⁹, the most widely used Hg inventory. This difference arises because our study includes additional emissions from sources such as agricultural burning, industrial solid waste, and aviation and navigation. Moreover, our study offers more detailed time scales (62 years vs. 2 years), higher spatial resolution ($0.1^\circ \times 0.1^\circ$ vs. $0.25^\circ \times 0.25^\circ$) and greater emission source precision (121 vs. 50) compared to the GMA 2018 (Supplementary Text 3). Our temporal trends are consistent with Streets et al.^{17,39}, though their studies did not account for detailed spatial distribution (Supplementary Fig. 1). As the largest emission sector, our ASGM estimate is also within the range of previous estimates^{17,36,38,39,47} (727–838 Mg during the 2010s, Supplementary Figs. 2 and 3). The largest discrepancy is in the waste incineration sector, with our estimate at 63 Mg—three-fold larger than that of GMA¹⁹—probably due to differences in activity data⁵¹. Additionally, the GMA inventory does not cover sectors such as agricultural burning and the incineration of certain wastes, including industrial waste²⁷, whereas these are included in our work. Comparing our results with previous studies increases confidence in our estimates and reinforces the belief that the Minamata Convention may have the potential to curb the growth in global anthropogenic Hg emissions.

Declining mercury emissions in the Global North and China

Over the past six decades, the spatiotemporal distribution of anthropogenic Hg emissions has substantially changed worldwide (Fig. 2). In 2021, China, India, Indonesia, Peru, and Brazil emitted 566, 264, 148, 144, and 85 Mg of Hg, respectively, accounting for half of the global emissions (Supplementary Figs. 4 and 5). In contrast, in 1960, these five countries only accounted for 19% of global emissions, with the Global North being the main emitter at that time (Fig. 3). We divided the globe into ten regions following published literature (Supplementary Data 1),

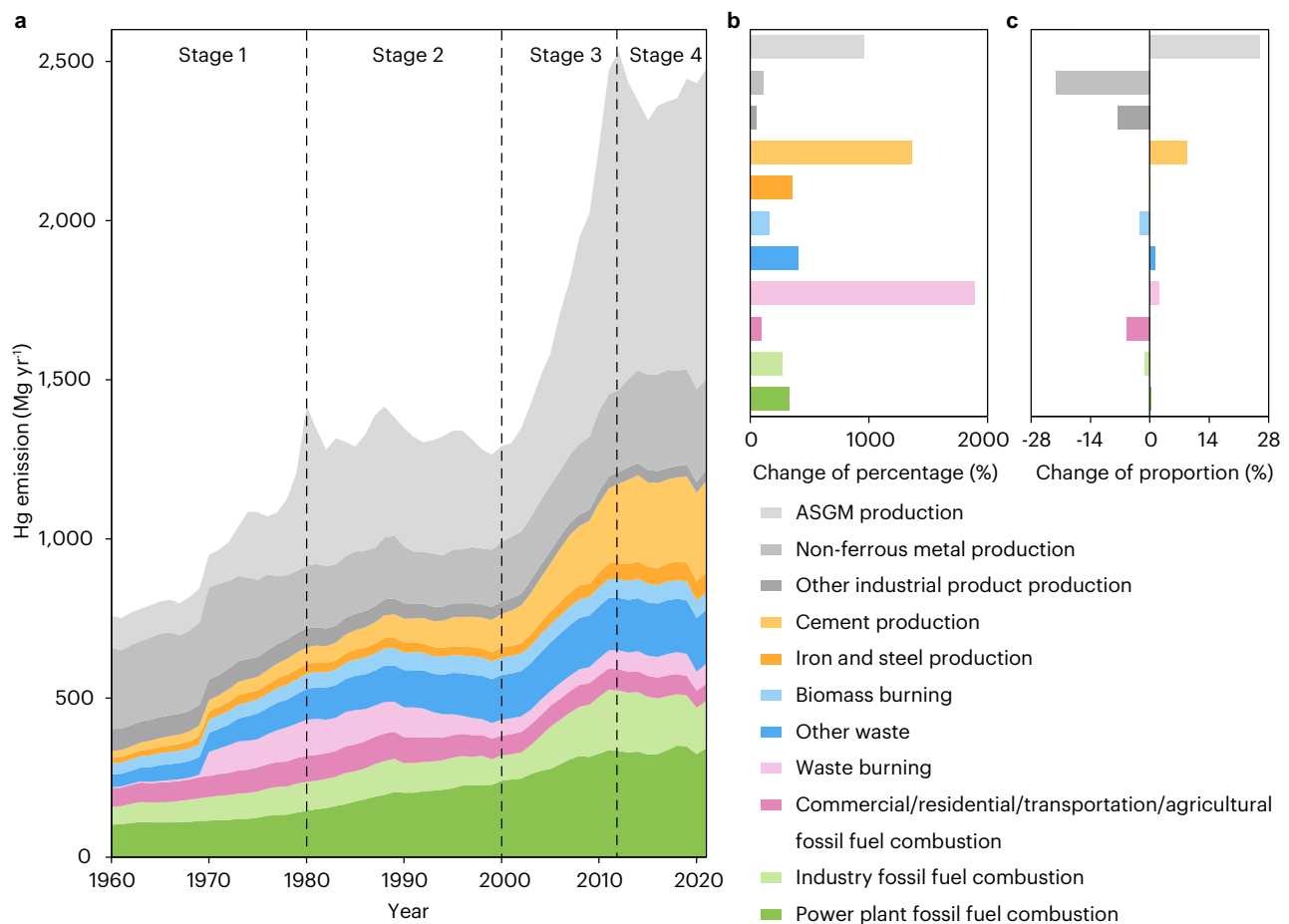


Fig. 1 | Global anthropogenic Hg emissions to the atmosphere from 1960 to 2021. a Global anthropogenic Hg emissions by sector from 1960 to 2021. **b** Increases in the emissions of each sector from 1960 to 2021. **c** Changes in the proportion of each sector in global emissions from 1960 to 2021. A detailed catalog

for each sector is available in Supplementary Table 1. Detailed annual emissions for each sector are available in Supplementary Table 2. The uncertainty of Hg emissions worldwide and from each sector is presented in Supplementary Figs. 1 and 2, respectively. ASGM - artisanal and small-scale gold mining.

with the Global North including developed countries mainly in Europe, Northern America, and Oceania^{30,52}.

In 1960, the Global North accounted for nearly half of global emissions. However, by 2021, this share had decreased to only 10% (Fig. 3a), with a decline in annual emissions from 512 Mg to 260 Mg over the past thirty years. This reduction is greatly driven by decreased fossil fuel combustion³⁹, which alone accounts for a reduction of 134 Mg (Fig. 4), achieved through policies promoting renewable energy and enhancing energy efficiency^{53,54} (Supplementary Text 1). Waste burning was the second largest contributor, with a 63 Mg reduction in emissions for the last thirty years (Fig. 4), mainly due to improved waste management practices and stricter incineration regulations. Additionally, reductions in non-ferrous metal production and other industrial processes were the result of technological advancements and stricter emission controls⁵⁴.

The U.S. and Germany have seen the most significant emission reductions in the Global North over the past 62 years. U.S. emissions decreased from 123 Mg in 1980 to 32 Mg in 2021, and Germany's from 51 Mg to 15 Mg (Supplementary Figs. 4 and 5). Eastern and Central European countries showed a slightly different trend, with initial declines followed by a rebound after 2000 due to economic recovery and growth in countries like Russia (Fig. 4). In the 21st century, the pace of emission reductions has slowed in most Global North countries (Fig. 4), indicating that these countries have reached plateaus in Hg emission control, with diminishing marginal benefits from further reductions⁵⁵. Overall, most Global North countries have made significant contributions to the reduction of global anthropogenic Hg emissions. While several studies

have suggested this point^{17,18,33,35,36,38,50,56}, our analyses provide a more thorough examination at a much finer global spatial resolution with a unified estimation method.

Although China has been the world's largest emitter of anthropogenic Hg since 1971, its recent decline has played a key role in curbing global emission growth. China's Hg emissions peaked at 613 Mg in 2013 (546–750 Mg, interquartile range), nine-fold greater than that in 1960 (Fig. 4). Subsequently, it began to decline, contributing to 75% of the total reductions in the Global North and China during 2013–2021. Recent localized emission inventories from China confirm this trend^{41,57}. Industrial fossil fuel combustion is the main driver of these reductions (Fig. 4). Since 2013, residential fossil fuel combustion, biomass burning, cement production, and waste disposal sectors also show downward trends, while emissions from iron and steel production and power plant fossil fuel combustion are still growing. Overall, China's air pollution control measures, such as the ultralow emission upgrades in key industries^{25,41,58}, have greatly decoupled Hg emissions from economic development (Supplementary Text 1). However, China's current Hg emissions remain substantial, accounting for a quarter of the global total, indicating significant potential for further reductions.

Global mercury emission hotspots shifting southward

Our analyses show that efforts by the Global North and China to reduce anthropogenic Hg emissions have been offset by rapid growth in the Global South. Over the past 62 years, global Hg emission hotspots have significantly shifted toward the Global South (Fig. 3b), with Latin America, Africa, South and Southeast Asia experiencing rapid

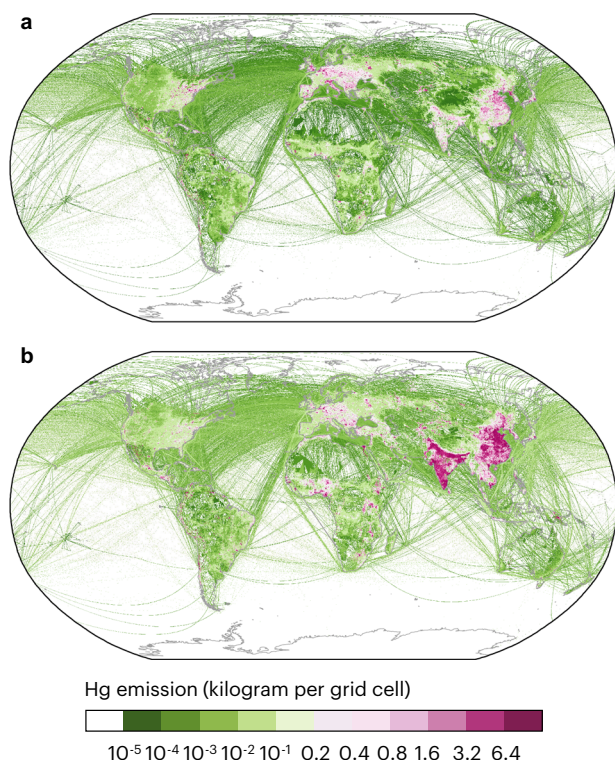


Fig. 2 | Spatial distribution of global anthropogenic Hg emissions. Data is presented for 1960 (a) and 2021 (b). The map is sourced from National Platform for Common GeoSpatial Information Services (<https://www.tianditu.gov.cn/>), labelled as GS(2021) 5450.

increases (Fig. 3a). In 2021, despite representing only one-fifth of the global economy⁵⁹, the Global South (excluding China) constituted two-thirds of global emissions. Therefore, controlling Hg emissions in the Global South should be a priority.

Major drivers of Hg emission growth vary substantially among different Global South countries and regions. Latin America, Sub-Saharan Africa, and Southeast Asia are the three major regions for Hg emissions after East Asia, with increases over the past 62 years of 400%, 200%, and 700% respectively (Fig. 4). In these regions, ASGM accounts for up to 70% of the recent increase in Hg emissions, with the country Peru, Indonesia, and Colombia have contributed most to the growth in global ASGM Hg emissions (Supplementary Fig. 4). These regions showed a slight decrease in Hg emissions from 2012 to 2015, mainly due to the short-term decline in ASGM emissions caused by falling gold prices⁶⁰. However, with the recovery of international gold prices after 2015⁶¹, ASGM Hg emissions in these regions have rebounded (Fig. 4).

Most industrial sectors in Latin America, Sub-Saharan Africa, and Southeast Asia have experienced rapid growth in Hg emissions, with declines only in the non-ferrous metal production sector (Fig. 4). Aside from ASGM, non-ferrous metal production, power plant fossil fuel combustion, and other waste are the largest sectors of Hg emissions in those areas, with changes over the past 62 years of -32%, 1300%, and 540%, respectively (Fig. 4). In Latin America, emissions from non-ferrous metal production have declined in recent years, mainly due to reduced copper smelting. In contrast, this sector has grown rapidly in Sub-Saharan Africa, primarily due to increased large-scale gold mining production. Historically, South Africa was the largest anthropogenic Hg emissions country in the Global South. However, its emissions have fallen to 29% of 1960 levels by 2021, thanks to a reduction in large-scale gold mining production (Supplementary Figs. 4–6).

South Asia has different major drivers for its rapid increase in Hg emissions compared to the aforementioned regions^{39,54}. It has

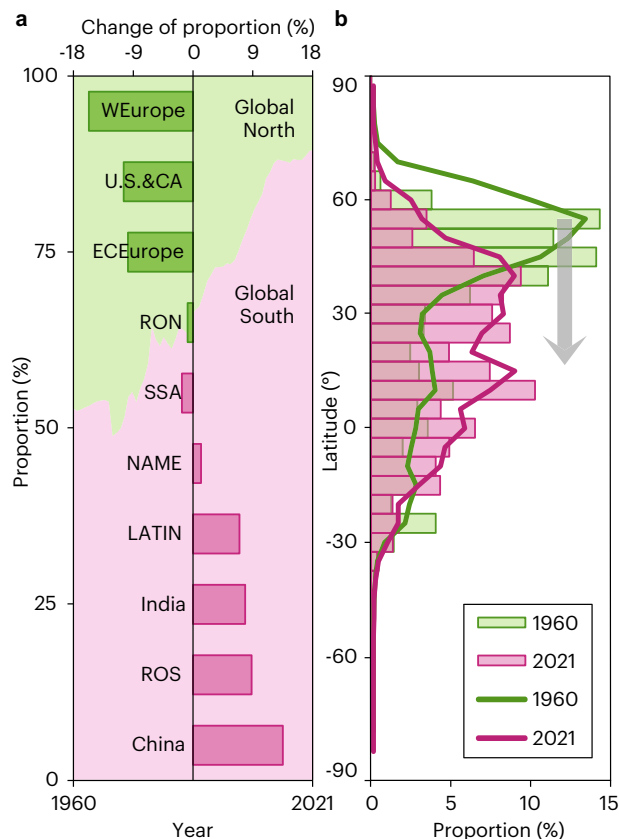


Fig. 3 | Spatiotemporal shifts in anthropogenic Hg emissions worldwide from 1960 to 2021. a Shifts in the proportion of global emissions contributed by ten regions from 1960 to 2021. b Latitudinal shifts in Hg emissions from 1960 to 2021. In panel b, bars represent the sum of all anthropogenic Hg emissions in each latitudinal interval, lines represent the latitudinal trends of Hg emissions, and the gray arrow represents the direction of movement of the emission hotspots. WEurope - Western Europe, ECEurope - Eastern and Central Europe, U.S.&CA - United States and Canada, RON - the rest of the Global North, SSA - Sub-Saharan Africa, NAME - Northern Africa and the Middle East, LATIN - Latin America, ROS - the rest of the Global South.

experienced the fastest Hg emissions growth worldwide, rising by 1200% over the past 62 years—four-fold greater than the global average (Fig. 4). In India, the major country in South Asia, emissions from all sectors have increased continuously since 1960, with fossil fuel combustion growing the fastest. Currently, India's anthropogenic Hg emissions far exceed those of other countries, ranking second only to China (Supplementary Fig. 4). In key driving sectors such as power plant, industrial fossil fuel combustion, and cement production, mitigation measures have been limited and insufficient to offset emissions from rapid economic growth^{34,62} (Supplementary Fig. 5). If still uncontrolled, India could soon become the world's leading emitter of anthropogenic Hg (Supplementary Text 2).

Implications for global mercury pollution and emission reductions

In this study, we developed a high-resolution dataset detailing 62 years of spatiotemporal variations in global anthropogenic atmospheric Hg emissions. Our findings show that emission hotspots have comprehensively shifted southward. Despite significant reduction efforts made by the Global North and China, these have been entirely offset by rapid increases in the Global South. Currently, global Hg emission control is at a critical juncture, with emission increases from the Global South, excluding China, now driving global trends.

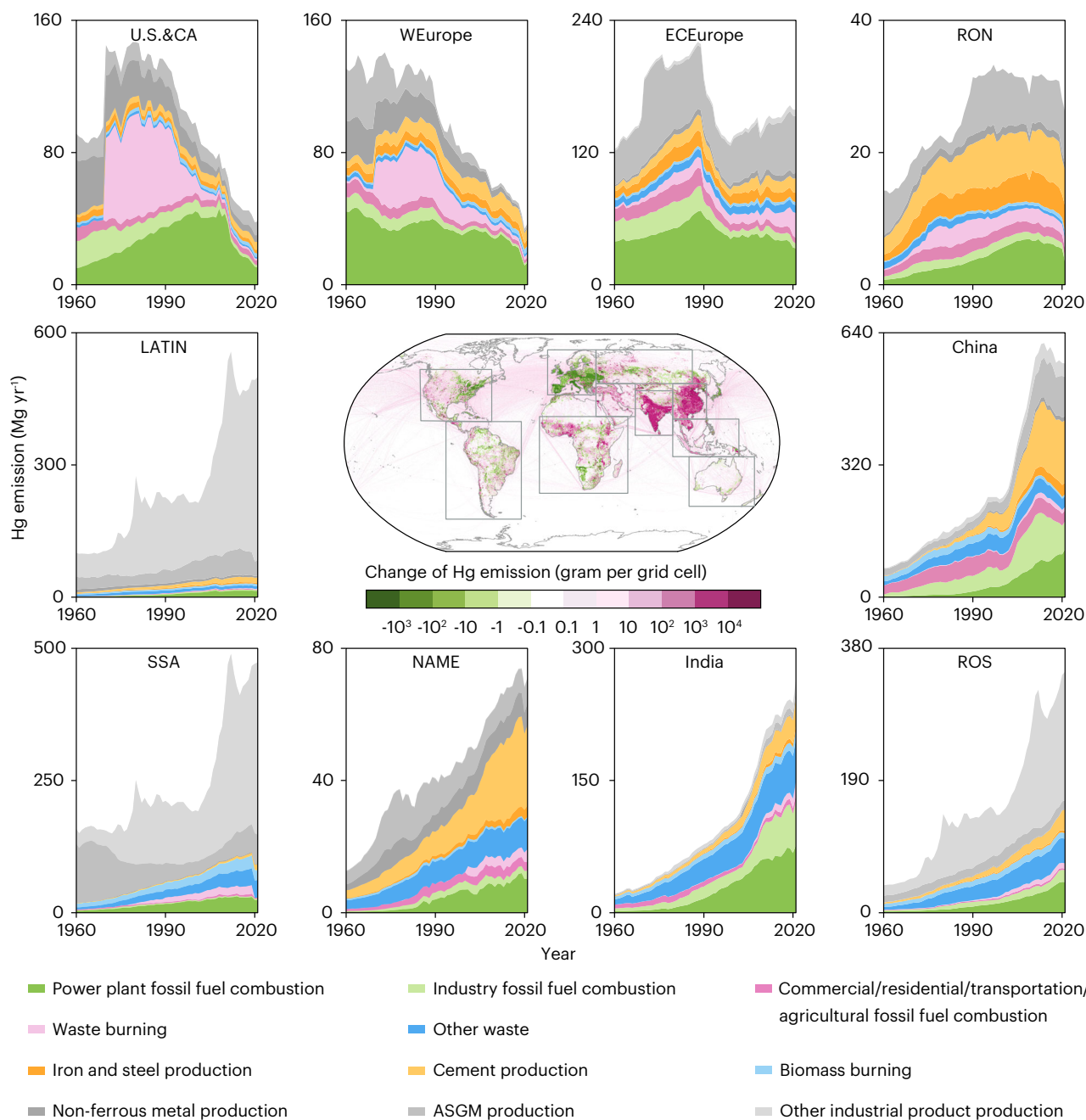


Fig. 4 | Regional anthropogenic Hg emissions by sector from 1960 to 2021. WEurope - Western Europe, ECEurope - Eastern and Central Europe, U.S.&CA - United States and Canada, RON - the rest of the Global North, SSA - Sub-Saharan Africa, NAME - Northern Africa and the Middle East, LATIN - Latin America, ROS - the rest of the Global South. ASGM - artisanal and small-scale gold mining. Annual

emissions of Hg by world region are available in Supplementary Table 3. The emissions of major countries are presented in Supplementary Fig. 5. The map is sourced from National Platform for Common GeoSpatial Information Services (<https://www.tianditu.gov.cn/>), labelled as GS(2021) 5450.

Without immediate action to reduce emissions, global Hg emissions will continue to rise rapidly, posing greater threats to ecosystems and human health.

Since the signing of the Minamata Convention in 2013, global anthropogenic Hg emissions have temporarily ceased to rapid increase. However, the current North-South emission balance could soon be disrupted. Based on two assumed scenarios, we project that global emissions could reach 2800–3600 Mg by 2030 (Supplementary Text 2). This increase due to rapid growth in the Global South outpacing reduction in the Global North and China, coupled with rising in future gold demand⁴⁷. Despite large uncertainties in ASGM⁶³, this extrapolation reinforces the fact that Hg emissions from the Global

South could drive global emissions to higher levels³⁹. Focus is needed on countries such as India and Indonesia.

The growth of global Hg emissions and the southward shift of emission hotspots have significant implications on environmental Hg pollution. Our results explain the decline in atmospheric Hg concentrations in Western countries over the past thirty years^{18,24,64} and in China during the past decade⁶⁵, as well as the rise at some monitoring stations in the Global South⁶⁶. If not promptly controlled, Global South's emissions could completely offset the decline in atmospheric Hg concentrations in Europe, the U.S., and China. High atmospheric Hg emissions are often accompanied by large amounts of Hg released into aquatic ecosystems⁶⁷, particularly in rivers, lakes, and coastal seas in

current hotspot areas⁶⁸. This raises concerns about greater Hg accumulation in food webs, increasing the exposure risk to Hg-contaminated seafood for local inhabitants¹⁴. Furthermore, the southward shift of emission hotspots will alter global Hg deposition patterns. Arctic ecosystems have historically been impacted by anthropogenic Hg emissions. Similarly, ongoing increases in Hg emissions from the Global South could transport more Hg to the Antarctic via atmospheric and oceanic currents, posing potential threats to those ecosystems. These changes highlight the urgency of controlling Hg emissions, requiring international collaboration to ensure the implementation of the Minamata Convention worldwide.

As previously mentioned, to enhance the implementation of the Minamata Convention, we recommend strengthening ASGM management in the Global South, particularly in Latin America, Sub-Saharan Africa, and Southeast Asia. Governments could incentivize alternative livelihoods, provide training on sustainable mining practices, and improve access to financial resources for miners transitioning away from Hg use. Furthermore, international partnerships could offer technical and financial support to develop local capacities for Hg-free mining technologies. China's declining emissions trend demonstrates that significant reductions are possible by controlling sectors like power plant combustion and metal smelting^{41,57}. Its air pollution control strategies—comprehensive policies, strict enforcement, and technological innovation—provide valuable insights for other developing countries⁵⁸ (Supplementary Text 1). However, China still emits large amounts of Hg and should tighten pollution control, particularly in cement production and fossil fuel combustion^{25,41,57}, by setting stricter emission limits, improving monitoring, and investing in advanced abatement technologies. India's Hg emission pattern mirrors China's past, and without intervention, it could increase dramatically, presenting a major uncertainty in future global Hg control. India should implement stringent regulations in its power and industrial sectors, phase out outdated technologies, and adopt cleaner energy sources. Moreover, successful reduction measures from North America and Europe, such as end-of-pipe measures, energy efficiency improvements, and transitioning to cleaner energy sources, should be shared with developing countries to enhance their Hg emission reduction capabilities. These actions are crucial for achieving significant Hg emission reductions, mitigating its harmful impacts, and safeguarding global ecosystems and public health.

The uncertainty of global annual Hg emissions based on Monte Carlo simulations ranges from −30% to 40% (interquartile range, Supplementary Fig. 1). The PKU-FUEL's point source data used in this study reduces the coefficient of variation of activity data, thereby reducing overall uncertainty⁴⁶. ASGM has the largest uncertainty among emission sectors, contributing 62% of the total in 2021 (Supplementary Text 3). Reducing the uncertainty is challenging due to the unregulated ASGM activities and reliance on data from organizations like UNEP¹⁹. Other emission sectors also face limitations due to data availability. Although our database is comprehensive, the underrepresentation of some sectors or missing activity data may increase uncertainty. More broadly, these issues are common across global pollutant emission inventories, particularly in the Global South countries. As more reliable statistics and monitoring data become available, updating our estimates will be essential.

Finally, we emphasize that this 62-year high-resolution assessment enhances understanding of the global Hg cycle and its impact on humans. Our refined gridded assessments are useful for forcing atmospheric chemistry models^{5,18,21,31}. They can help improve the quantification of anthropogenic Hg emissions' contribution to transboundary transport⁶⁹, as well as land-air and air-sea exchange fluxes of Hg, which remain poorly constrained in models^{8,65,70}. Additionally, our long-term assessment helps better evaluate the risks of rapid Hg emission increases in the Global South and understand the health risks caused by historical emissions in the Global North. Moreover, this

assessment provides a foundation for the new Earth system models with higher spatiotemporal resolution, enabling more accurate and detailed simulations of global Hg distribution and dynamics. This will help to illuminate the complex dynamics between climate change and the anthropogenic Hg cycle. In conclusion, this study reveals that global anthropogenic Hg emission control is at a critical juncture and highlights the southward shift of emission hotspots. Future success in reducing Hg pollution may depend on actions taken in the Global South.

Methods

Inventory development

This study aims to enhance the spatiotemporal resolution and precision of emission sectors in the inventory. We utilized the widely adopted bottom-up method to compile a global inventory of anthropogenic atmospheric Hg emissions^{6,36,38,39,46,47}. By integrating recent scientific literature, monitoring data, and advanced computational methods, we developed the most detailed high-resolution global anthropogenic Hg emission inventory to date, covering the longest time span on a year-by-year basis and the most comprehensive range of sectors. Annual emissions are calculated using the following formula:

$$E_t = \sum_{i,j} (EF_{i,j,t} \times A_{i,j,t}) \quad (1)$$

where E represents the amount of anthropogenic Hg emissions (Mg yr^{-1}), EF is the emission factor (Mg Mg^{-1}), A is the activity data (Mg yr^{-1}), i is the country or region, j is the emission sector, and t is the time.

In this study, we meticulously calculated anthropogenic Hg emissions from 121 detailed emission sectors across 225 countries and regions over a 62-year period from 1960 to 2021. Emission sectors were primarily categorized according to the GMA inventory²⁷, with updates and supplements from the detailed PKU-FUEL database⁷¹ (Supplementary Text 4). The anthropogenic sectors considered in this study can be categorized into three major groups:

1. Fuel combustion sector: this includes fossil fuel combustion in power plants, industry, resident, commerce, transportation, and agriculture; biomass burning; and waste incineration.
2. Non-combustion sector: this includes the production of non-ferrous metals (aluminum, copper, lead, zinc, large-scale gold, mercury), iron and steel production, cement production, crude oil refining, chlor-alkali production, and uncontrolled waste landfills.
3. Artisanal and small-scale gold mining (ASGM).

Biomass burning, newly introduced in the GMA 2018 inventory, has garnered increased attention in recent years. While the GMA 2018 broadly categorized it as a single sector, we conducted a detailed study on 16 types of biomass fuel emissions (Supplementary Table 1). ASGM is the largest emission sector globally. However, due to its illegality and the prevalence of mining in underdeveloped regions⁶⁰, statistical data is often lacking, leading to large uncertainties in emission calculations. Given this, we have separately listed ASGM in Supplementary Text 5. Overall, this study covers 121 detailed Hg emission sectors, including 105 combustion sources and 16 non-combustion sources.

Activity data

The activity data for all combustion sectors and some non-combustion sectors in this study were collected from the PKU-FUEL database. This database is one of the most updated and detailed sources available, providing extensive data from 1960 to 2021 with a high spatial resolution of $0.1^\circ \times 0.1^\circ$. It has three main features: (1) generating global fuel consumption data at a $0.1^\circ \times 0.1^\circ$ resolution, based on detailed sub-national administration energy data disaggregated by counties (China, USA, and Mexico), $0.5^\circ \times 0.5^\circ$ (European countries), or

provinces/states (India, Canada, Turkey, Australia, Brazil)⁴⁵; (2) updating detailed residential energy consumption data in rural China through energy surveys and fuel measurements involving over 34,000 households⁷², which revealed inaccuracies in the International Energy Agency's report on China's rural biomass fuel consumption; (3) providing detailed statistics on agricultural sectors and biomass fuel combustion data^{51,73}, which are significant sectors of Hg emissions. Previous inventories, such as the GMA 2018, have not fully quantified the agricultural combustion sector due to a lack of data²⁷. PKU-FUEL has been widely used in the emission research of important greenhouse gases and air pollutants such as carbon dioxide, nitrogen oxides, atmospheric particulate matter, and polycyclic aromatic hydrocarbons^{45,51,73–76}. Therefore, the PKU-FUEL data is crucial for updating this inventory.

The remaining activity data were obtained from various sources, including the World Steel Association⁷⁷, the United States Geological Survey⁷⁸, national statistical reports, and literature statistics. ASGM's activity data, which are not directly available, were estimated using existing information such as gold prices and the artisanal and small-scale mining population, following the method by Seccatore et al., 2014⁶⁰ (Supplementary Text 5).

Emission factor

The emission factor is the coefficient of Hg emissions per unit activity of the emission sector, primarily determined by the Hg content of the fuel or raw material and the emission reduction efficiency of APCDs^{39,41,47,57}. Hg content is generally influenced by geological origins and processing methods^{33,79,80}. Abatement efficiency refers to the proportion of Hg emissions that can be reduced by specific processes or control technologies. This efficiency depends on factors such as the form of Hg, characteristics of the emission sector, and the operational conditions and usage rates of reduction equipment^{39,41,47,57}.

We applied varying methods for the emission factors at different time periods (Supplementary Texts 6 and 7). For the most recent year 2021, emission factors were primarily derived from the UNEP Toolkit for Identifying and Quantifying Mercury Emissions, version 1.5⁸¹. However, due to the lag in UNEP data updates, recent research literature and industrial bulletins were also reviewed to obtain the latest emission factors (Supplementary Tables 4–6). The specific calculation formula for the emission factor is as follows:

$$EF_{i,j,t,m} = C_{i,j} \times \sum_k F_{j,k,t} \times (1 - R_k) \times Q_{j,k,m} \quad (2)$$

where m is the Hg species, k is the combination type of APCDs, F is the application rate, C is the average Hg content in fuel or raw material (g Mg^{-1}), R is the Hg removal rate, and Q is the proportion of the corresponding species of Hg.

Quantifying historical emissions of anthropogenic Hg requires accounting for temporal variations in emission factors. Over time, process technology tends to improve, and the application rate of APCDs gradually increases, enhancing pollution control^{39,41,47,57}. However, annual historical data on emission factors are often poorly documented. Our study applied a sigmoid curve method developed by Streets et al.¹⁷ to simulate the impact of technological changes on emission factors by varying the application rates of different APCDs combinations over time (Supplementary Text 7). This approach has been widely used to estimate historical and future emissions of pollutants such as black carbon⁸² and organic carbon aerosols⁸³. The following equation was used to estimate the change of anthropogenic Hg abatement factor over time:

$$y_{i,j,t} = (a_{i,j} - b_{i,j}) e^{-\left(\frac{t^2}{s_{i,j}^2}\right)} + b_{i,j} \quad (3)$$

where y is the emission reduction factor (g Mg^{-1}), a is the emission factor under the worst historical conditions (g Mg^{-1}), b is the best achievable emission factor (g Mg^{-1}), and s is the shape parameter of the sigmoid curve. The value of y at any point in time is estimated by selecting the values of parameters a , b , and s corresponding to the known technology or inferred development path (Supplementary Data 2).

In the calculation process, all 225 countries and regions were categorized into five groups (group 1–5) based on technological development levels^{17,27} (Supplementary Data 1), with corresponding sigmoid curves provided. The waste sector was classified separately according to the GMA 2018 setting considering different waste management policies of different countries. Supplementary Data 2 provides parameter values for the sigmoid curves of each Hg emission sector.

For detailed analysis, countries and regions were also grouped into ten regional classifications in the discussion, following the approach of previous studies⁵² (Supplementary Data 1): China, India, ROS (the rest of the Global South), LATIN (Latin America), SSA (Sub-Saharan Africa), NAME (Northern Africa and the Middle East), ECEu (Eastern and Central Europe), WEu (Western Europe), RON (the rest of the Global North), U.S. & CA (United States and Canada). The first seven are all developing countries, which make up the Global South, while the last four make up the Global North, which are mostly developed countries.

Additionally, different Hg species exhibit significant differences in environmental behavior and ecological toxicity. Understanding the distribution and emissions of Hg species in various sectors is crucial for Hg reduction. Hg is released into the atmosphere in three forms: gaseous elemental Hg (Hg^0), gaseous oxidized Hg (Hg^{2+}), and particle-bound Hg (Hg^p). We estimated historical trends in the proportion of anthropogenic Hg species emissions globally (Supplementary Texts 6 and 8). The distribution profile of Hg species in different sectors was based on previous work of Streets et al.³⁹ and Wu et al.⁵⁷ (Supplementary Table 7).

Spatial analysis

This study spatially interpolated anthropogenic Hg emission data as a detailed, long-term (1960–2021), high spatial resolution ($0.1^\circ \times 0.1^\circ$) gridded inventory for 121 sectors (Supplementary Text 9). The gridding method primarily relied on the high-resolution energy inventory from the PKU-FUEL team⁷¹. Hg emission sources were categorized into point and non-point sources. For point sources, emissions were allocated directly into spatial grids using precise geographic coordinates from relevant industry associations⁴⁵ (Supplementary Table 8). For example, cement production emissions were distributed based on cement facilities locations, petroleum catalytic cracking emissions on refinery locations, non-ferrous metal production on specific mine data points, and iron and steel production on industrial coal consumption. ASGM emissions were based on EDGARv4^{36,38} and recent national reports⁸⁴.

For non-point combustion sources, the PKU-FUEL team used a variety of proxies such as total population, rural population, and GDP to disaggregate sub-national level (such as county, city, province, state, etc.) or point-based or surveyed gridded fuel consumption into $0.1^\circ \times 0.1^\circ$ grid data⁴⁵ (Supplementary Table 8). Notably, the PKU-FUEL data adopted in this study is based on local data. Compared with previous inventories downscaled country emissions by population density, this method can greatly reduce the uncertainty caused by the spatial distribution bias due to unequal per capita fuel consumption within countries^{80,84}.

Future prediction

We predicted global Hg emissions by 2030 under a business-as-usual scenario. ASGM plays an important role in global Hg emissions.

However, ASGM Hg emissions have large uncertainties⁶³. Following published literature^{47,63,85}, we set two ASGM Hg emission scenarios, i.e., high and low emissions. In the high-emission scenario, Hg emissions were predicted based on gold price fluctuations for countries not among the 46 that have signed the Minamata Convention National Action Plans (NAPs)⁸⁴, assuming ASGM production driven by gold prices will continue in non-NAP countries, while NAP countries will reduce ASGM activities. The low-emission scenario, following Streets et al.⁸⁵, assumes constant ASGM emissions for all countries, due to limited data on temporal variation in Hg emissions associated with artisanal gold extraction. For other sectors, Hg emissions were calculated using each country's annual average change rates from 2013 to 2021 under the business-as-usual scenario^{47,63}.

Uncertainty analysis

This study employed Monte Carlo simulation to assess the uncertainty^{39,41,51,57}. Specifically, emissions from different sectors were recalculated 10,000 times by randomly drawing all inputs from given distributions (Supplementary Text 3). Key input parameters included uncertainty in activity data, Hg content in fuel or raw materials, and APCDs' Hg removal efficiency⁸⁶. Consistent with previous studies^{36,38}, activity data were assumed to be evenly distributed. Apart from the resident biomass combustion source with a coefficient variation of 10%, other sectors were set at 5%, which is lower than previous studies due to the higher precision and accuracy of PKU-FUEL activity data^{51,87}. For ASGM, lacking public data, activity data uncertainty ranges were assumed to be $\pm 30\%$, 50% , 75% , and 100% based on data quality in different countries, according to the GMA 2018²⁷. This inventory updates data for many developing countries owing to the implementation of Minamata Convention⁸⁴, significantly improving ASGM data quality and reducing uncertainties (Supplementary Text 5).

Hg concentrations in fuels or raw materials followed a log-normal distribution^{45,80}, as further confirmed by measurements reported in the literature from China⁵⁷. For the distribution characteristics of APCDs' Hg removal efficiency in 2021, we referred to Wu et al.⁵⁷, which fit either a Weibull or a normal distribution (Supplementary Table 5). Long-term annual emission factor data lacked uncertainty information, so these emission factors were assumed to follow a triangular distribution, consistent with previous studies³⁷. Ultimately, Monte Carlo simulations generated probability distributions of annual anthropogenic Hg emissions from each sector, globally and by country or region, from 1960 to 2021. The interquartile range was used as an indicator of uncertainty.

Uncertainty in future predictions mainly arises from the potential variations in Hg emissions under different scenarios. In the high-emission scenario, non-signatory countries of the Minamata Convention are expected to see increased ASGM activities driven by rising gold prices⁸⁴, leading to significantly higher Hg emissions. In contrast, the low-emission scenario, constrained by limited data, assumes constant ASGM emissions across all countries⁸⁵, resulting in much lower estimates. This creates a broad uncertainty range between the maximum and minimum predicted values. Additionally, Hg emissions from other sectors are projected based on historical trends, which could shift due to future economic, political, or technological changes, further increasing uncertainty. Consequently, future emission levels are not fixed and could fluctuate widely, reflecting the variability of future scenarios.

Limitations and future improvement directions

While we developed a comprehensive high-spatiotemporal-resolution dataset, several limitations remain. First, the accuracy of Hg emission factors needs improvement, as variations in economic levels, industrial activities, and APCDs across regions result in an incomplete reflection of actual emissions⁸⁸. This issue is common across nearly all global pollutant emission inventories⁸⁹, not just Hg. Second, the quality and availability of activity data, especially in developing countries and

regions, is a major limitation⁹⁰. Inconsistencies in data collection methods or databases across regions also contribute to uncertainty⁹¹. Although we have included previously unconsidered emission sectors for Hg, such as agricultural combustion, aviation, and shipping, our inventory might still not fully capture emerging or less-studied emission sources.

Additionally, the Hg emission projections in this study are preliminary and lack detailed scenario analyses, as that was beyond the scope of this research. Considering the complexity and dynamics of future economic development, technological advancements, market dynamics, policy implementation, and climate change impacts, these predictions should be interpreted cautiously. We recommend that future research incorporate sensitivity analyses or scenario modeling to explore a broader range of possible outcomes. These limitations are common in emission inventory studies. Addressing these limitations will require continuous efforts to improve data transparency, emission monitoring, and modeling practices, alongside strengthened international cooperation to enhance the accuracy and reliability of Hg emission inventories.

Data availability

All processed data are available in the article, Supplementary Information, or Figshare repository (<https://doi.org/10.6084/m9.figshare.26539714>)⁹².

References

- Mason, R. P. et al. Mercury biogeochemical cycling in the ocean and policy implications. *Environ. Res.* **119**, 101–117 (2012).
- Driscoll, C. T., Mason, R. P., Chan, H. M., Jacob, D. J. & Pirrone, N. Mercury as a global pollutant: sources, pathways, and effects. *Environ. Sci. Technol.* **47**, 4967–4983 (2013).
- Outridge, P. M., Mason, R. P., Wang, F., Guerrero, S. & Heimbürger-Boavida, L. E. Updated Global and Oceanic Mercury Budgets for the United Nations Global Mercury Assessment 2018. *Environ. Sci. Technol.* **52**, 11466–11477 (2018).
- Zhou, J., Obrist, D., Dastoor, A., Jiskra, M. & Ryjkov, A. Vegetation uptake of mercury and impacts on global cycling. *Nat. Rev. Earth Environ.* **2**, 269–284 (2021).
- Zhang, Y. et al. An updated global mercury budget from a coupled atmosphere-land-ocean model: 40% more re-emissions buffer the effect of primary emission reductions. *One Earth* **6**, 316–325 (2023).
- Pirrone, N. et al. Global mercury emissions to the atmosphere from anthropogenic and natural sources. *Atmos. Chem. Phys.* **10**, 5951–5964 (2010).
- Araujo, B. F. et al. Mercury isotope evidence for Arctic summertime re-emission of mercury from the cryosphere. *Nat. Commun.* **13**, 4956 (2022).
- Yue, F. et al. The Marginal Ice Zone as a dominant source region of atmospheric mercury during central Arctic summertime. *Nat. Commun.* **14**, 4887 (2023).
- Hammerschmidt, C. R., Fitzgerald, W. F., Lamborg, C. H., Balcom, P. H. & Visscher, P. T. Biogeochemistry of methylmercury in sediments of Long Island Sound. *Mar. Chem.* **90**, 31–52 (2004).
- Seelen, E. et al. Dissolved organic matter thiol concentrations determine methylmercury bioavailability across the terrestrial-marine aquatic continuum. *Nat. Commun.* **14**, 6728 (2023).
- Lavoie, R. A., Jardine, T. D., Chumchal, M. M., Kidd, K. A. & Campbell, L. M. Biomagnification of mercury in aquatic food webs: a world-wide meta-analysis. *Environ. Sci. Technol.* **47**, 13385–13394 (2013).
- Motta, L. C. et al. Mercury isotopic evidence for the importance of particles as a source of mercury to marine organisms. *Proc. Natl Acad. Sci. USA* **119**, e2208183119 (2022).
- Bradley, M. A., Barst, B. D. & Basu, N. A review of mercury bioavailability in humans and fish. *Int. J. Environ. Res. Public Health* **14**, <https://doi.org/10.3390/ijerph14020169> (2017).

14. Lavoie, R. A., Bouffard, A., Maranger, R. & Amyot, M. Mercury transport and human exposure from global marine fisheries. *Sci. Rep.* **8**, 6705 (2018).
15. Raj, D. & Maiti, S. K. Sources, toxicity, and remediation of mercury: an essence review. *Environ. Monit. Assess.* **191**, 566 (2019).
16. Lindberg, S. et al. A synthesis of progress and uncertainties in attributing the sources of mercury in deposition. *Ambio* **36**, 19–33 (2007).
17. Streets, D. G. et al. All-time releases of mercury to the atmosphere from human activities. *Environ. Sci. Technol.* **45**, 10485–10491 (2011).
18. Zhang, Y. et al. Observed decrease in atmospheric mercury explained by global decline in anthropogenic emissions. *Proc. Natl Acad. Sci. USA* **113**, 526–531 (2016).
19. Arctic Monitoring and Assessment Programme (AMAP) and United Nations Environment Programme (UNEP). *Global Mercury Assessment 2018* (UNEP Chemicals Branch: Geneva, Switzerland, 2019).
20. Sprovieri, F., Pirrone, N., Ebinghaus, R., Kock, H. & Dommergue, A. A review of worldwide atmospheric mercury measurements. *Atmos. Chem. Phys.* **10**, 8245–8265 (2010).
21. Travnikov, O. et al. Multi-model study of mercury dispersion in the atmosphere: atmospheric processes and model evaluation. *Atmos. Chem. Phys.* **17**, 5271–5295 (2017).
22. Li, C. et al. Unequal Anthropogenic Enrichment of Mercury in Earth's Northern and Southern Hemispheres. *ACS Earth Space Chem.* **4**, 2073–2081 (2020).
23. Soerensen, A. L. et al. Multi-decadal decline of mercury in the North Atlantic atmosphere explained by changing subsurface seawater concentrations. *Geophys. Res. Lett.* **39** <https://doi.org/10.1029/2012gl053736> (2012).
24. Dastoor, A. et al. Arctic atmospheric mercury: sources and changes. *Sci. Total Environ.* **839**, 156213 (2022).
25. Liu, K. et al. Measure-specific effectiveness of air pollution control on China's atmospheric mercury concentration and deposition during 2013–2017. *Environ. Sci. Technol.* **53**, 8938–8946 (2019).
26. Feng, X. et al. Combating air pollution significantly reduced air mercury concentrations in China. *Natl Sci. Rev.* <https://doi.org/10.5194/egusphere-egu24-14646> (2024).
27. Arctic Monitoring and Assessment Programme (AMAP) and United Nations Environment Programme (UNEP). *Technical Background Report to the Global Mercury Assessment 2018* (UNEP Chemicals Branch: Geneva, Switzerland, 2019).
28. Slemr, F. et al. Comparison of mercury concentrations measured at several sites in the Southern Hemisphere. *Atmos. Chem. Phys.* **15**, 3125–3133 (2015).
29. Slemr, F. et al. Atmospheric mercury in the Southern Hemisphere – Part 1: trend and inter-annual variations in atmospheric mercury at Cape Point, South Africa, in 2007–2017, and on Amsterdam Island in 2012–2017. *Atmos. Chem. Phys.* **20**, 7683–7692 (2020).
30. World Economic and Financial Surveys World Economic Outlook Database-WEO Groups and Aggregates Information. (International Monetary Fund 2023, accessed May 20, 2023); <https://www.imf.org/en/Publications/WEO/weo-database/2023/April/groups-and-aggregates>.
31. Corbitt, E. S., Jacob, D. J., Holmes, C. D., Streets, D. G. & Sunderland, E. M. Global source-receptor relationships for mercury deposition under present-day and 2050 emissions scenarios. *Environ. Sci. Technol.* **45**, 10477–10484 (2011).
32. Pacyna, E. G., Pacyna, J. M., Steenhuisen, F. & Wilson, S. Global anthropogenic mercury emission inventory for 2000. *Atmos. Environ.* **40**, 4048–4063 (2006).
33. Pacyna, E. G. et al. Global emission of mercury to the atmosphere from anthropogenic sources in 2005 and projections to 2020. *Atmos. Environ.* **44**, 2487–2499 (2010).
34. Burger Chakraborty, L., Qureshi, A., Vadenbo, C. & Hellweg, S. Anthropogenic mercury flows in India and impacts of emission controls. *Environ. Sci. Technol.* **47**, 8105–8113 (2013).
35. Horowitz, H. M., Jacob, D. J., Amos, H. M., Streets, D. G. & Sunderland, E. M. Historical Mercury releases from commercial products: global environmental implications. *Environ. Sci. Technol.* **48**, 10242–10250 (2014).
36. Muntean, M. et al. Trend analysis from 1970 to 2008 and model evaluation of EDGARv4 global gridded anthropogenic mercury emissions. *Sci. Total Environ.* **494–495**, 337–350 (2014).
37. Ye, X. et al. Atmospheric mercury emissions from China's primary nonferrous metal (Zn, Pb and Cu) smelting during 1949–2010. *Atmos. Environ.* **103**, 331–338 (2015).
38. Muntean, M. et al. Evaluating EDGARv4.tox2 speciated mercury emissions ex-post scenarios and their impacts on modelled global and regional wet deposition patterns. *Atmos. Environ.* **184**, 56–68 (2018).
39. Streets, D. G. et al. Global and regional trends in mercury emissions and concentrations, 2010–2015. *Atmos. Environ.* **201**, 417–427 (2019).
40. Cai, X. et al. Establishment of high-resolution atmospheric mercury emission inventories for Chinese cement plants based on the mass balance method. *Environ. Sci. Technol.* **54**, 13399–13408 (2020).
41. Zhang, Y. et al. Improved anthropogenic mercury emission inventories for China from 1980 to 2020: toward more accurate effectiveness evaluation for the Minamata Convention. *Environ. Sci. Technol.* **57**, 8660–8670 (2023).
42. Schaefer, K. et al. Potential impacts of mercury released from thawing permafrost. *Nat. Commun.* **11**, 4650 (2020).
43. Sonke, J. E. et al. Global change effects on biogeochemical mercury cycling. *Ambio* **52**, 853–876 (2023).
44. Yuan, T. et al. Potential decoupling of CO₂ and Hg uptake process by global vegetation in the 21st century. *Nat. Commun.* **15**, 4490 (2024).
45. Wang, R. et al. High-resolution mapping of combustion processes and implications for CO₂ emissions. *Atmos. Chem. Phys.* **13**, 5189–5203 (2013).
46. Xiong, R. et al. Global brown carbon emissions from combustion sources. *Env. Sci. Ecotechnol.* **12**, 100201 (2022).
47. Pacyna, J. M. et al. Current and future levels of mercury atmospheric pollution on a global scale. *Atmos. Chem. Phys.* **16**, 12495–12511 (2016).
48. Francey, R. J. et al. Atmospheric verification of anthropogenic CO₂ emission trends. *Nat. Clim. Change* **3**, 520–524 (2013).
49. Kimijima, S., Sakakibara, M., Nagai, M. & Gafur, N. A. Time-series assessment of camp-type artisanal and small-scale gold mining sectors with large influxes of miners using LANDSAT imagery. *Int. J. Environ. Res. Public Health* **18** <https://doi.org/10.3390/ijerph18189441> (2021).
50. Fekete, H. et al. A review of successful climate change mitigation policies in major emitting economies and the potential of global replication. *Renew. Sust. Energ. Rev.* **137**, 110602 (2021).
51. Shen, H. et al. Global atmospheric emissions of polycyclic aromatic hydrocarbons from 1960 to 2008 and future predictions. *Environ. Sci. Technol.* **47**, 6415–6424 (2013).
52. Xiong, Y., Du, K. & Huang, Y. One-third of global population at cancer risk due to elevated volatile organic compounds levels. *npj Clim. Atmos. Sci.* **7** <https://doi.org/10.1038/s41612-024-00598-1> (2024).
53. Burmistrz, P., Kogut, K., Marczak, M. & Zwoździak, J. Lignites and subbituminous coals combustion in Polish power plants as a source of anthropogenic mercury emission. *Fuel Process. Technol.* **152**, 250–258 (2016).
54. Picciano, P. et al. Air quality related equity implications of U.S. decarbonization policy. *Nat. Commun.* **14**, 5543 (2023).
55. Samset, B. H., Fuglestad, J. S. & Lund, M. T. Delayed emergence of a global temperature response after emission mitigation. *Nat. Commun.* **11**, 3261 (2020).

56. Olson, C. I., Fakhraei, H. & Driscoll, C. T. Mercury emissions, atmospheric concentrations, and wet deposition across the conterminous United States: changes over 20 years of monitoring. *Environ. Sci. Technol. Lett.* **7**, 376–381 (2020).
57. Wu, Q. et al. Temporal trend and spatial distribution of speciated atmospheric mercury emissions in China during 1978–2014. *Environ. Sci. Technol.* **50**, 13428–13435 (2016).
58. Shi, Q. et al. Co-benefits of CO₂ emission reduction from China's clean air actions between 2013–2020. *Nat. Commun.* **13**, 5061 (2022).
59. International Monetary Fund. World Economic Outlook Database: April 2024 Edition. IMF. <https://www.imf.org/en/Publications/WEO/weo-database/2024/April> (2024).
60. Seccatore, J., Veiga, M., Origliasso, C., Marin, T. & De Tomi, G. An estimation of the artisanal small-scale production of gold in the world. *Sci. Total Environ.* **496**, 662–667 (2014).
61. World Gold Council (WGC). Gold investment digest; <https://www.gold.org> (accessed May 20, 2023).
62. Sharma, B. M., Bharat, G. K., Šebková, K. & Scheringer, M. Implementation of the Minamata Convention to manage mercury pollution in India: challenges and opportunities. *Environ. Sci. Eur.* **31** <https://doi.org/10.1186/s12302-019-0280-3> (2019).
63. Geyman, B. M. et al. Projecting global mercury emissions and deposition under the shared socioeconomic pathways. *Earths Future* **12**, e2023EF004231 (2024).
64. Cole, A. S. et al. Ten-year trends of atmospheric mercury in the high Arctic compared to Canadian sub-Arctic and mid-latitude sites. *Atmos. Chem. Phys.* **13**, 1535–1545 (2013).
65. Qin, X., Guo, Q., Martens, P. & Krafft, T. Mercury stable isotopes revealing the atmospheric mercury circulation: A review of particulate bound mercury in China. *Earth-Sci. Rev.* **250**, 104681 (2024).
66. Bieser, J., Angot, H., Slemr, F. & Martin, L. Atmospheric mercury in the Southern Hemisphere – Part 2: Source apportionment analysis at Cape Point station, South Africa. *Atmos. Chem. Phys.* **20**, 10427–10439 (2020).
67. Kocman, D. et al. Toward an assessment of the global inventory of present-day mercury releases to freshwater environments. *Int. J. Environ. Res. Public Health* **14** <https://doi.org/10.3390/ijerph14020138> (2017).
68. Liu, M. et al. Increases of total mercury and methylmercury releases from municipal sewage into environment in China and implications. *Environ. Sci. Technol.* **52**, 124–134 (2018).
69. Chen, L. et al. Trans-provincial health impacts of atmospheric mercury emissions in China. *Nat. Commun.* **10**, 1484 (2019).
70. Landis, J. D. et al. Quantifying soil accumulation of atmospheric mercury using fallout radionuclide chronometry. *Nat. Commun.* **15**, 5430 (2024).
71. Global Emission Modeling System (GEMS); <http://inventory.pku.edu.cn/home.html> (accessed July 10, 2024).
72. Chen, H. et al. Modeling temporal variations in global residential energy consumption and pollutant emissions. *Appl. Energy* **184**, 820–829 (2016).
73. Wang, R. et al. Trend in global black carbon emissions from 1960 to 2007. *Environ. Sci. Technol.* **48**, 6780–6787 (2014).
74. Huang, Y. et al. Quantification of global primary emissions of PM_{2.5}, PM₁₀, and TSP from combustion and industrial process sources. *Environ. Sci. Technol.* **48**, 13834–13843 (2014).
75. Huang, T. et al. Spatial and temporal trends in global emissions of nitrogen oxides from 1960 to 2014. *Environ. Sci. Technol.* **51**, 7992–8000 (2017).
76. Meng, W. et al. Improvement of a global high-resolution ammonia emission inventory for combustion and industrial sources with new data from the residential and transportation sectors. *Environ. Sci. Technol.* **51**, 2821–2829 (2017).
77. World Steel Association; <http://www.worldsteel.org> (accessed May 20, 2023).
78. U. S. Geological Survey (USGS). Commodity Statistics and Information; <http://minerals.usgs.gov/minerals/pubs/commodity> (accessed May 20, 2023).
79. Rytuba, J. J. Mercury from mineral deposits and potential environmental impact. *Environ. Geol.* **43**, 326–338 (2003).
80. Chen, Y. et al. Global mercury emissions from combustion in light of international fuel trading. *Environ. Sci. Technol.* **48**, 1727–1735 (2014).
81. UNEP. United Nations Environment Programme. *Toolkit for Identification and Quantification of Mercury Releases, Revised Inventory Level 2 Report* (UNEP Chemicals Branch: Geneva, Switzerland, 2018).
82. Bond, T. C. et al. Historical emissions of black and organic carbon aerosol from energy-related combustion, 1850–2000. *Glob. Biogeochem. Cycle* **21** <https://doi.org/10.1029/2006gb002840> (2007).
83. Streets, D. G., Bond, T. C., Lee, T. & Jang, C. On the future of carbonaceous aerosol emissions. *J. Geophys. Res. Atmos.* **109** <https://doi.org/10.1029/2004jd004902> (2004).
84. UNEP. *The Minamata Convention on Mercury 2021 National Reports*. (Minamata Convention, accessed May 20, 2023). <https://minamataconvention.org/en/parties/national-action-plans>.
85. Streets, D. G., Qiang, Z. & Ye, W. Projections of Global Mercury Emissions in 2050. *Environ. Sci. Technol.* **43**, 2983–2988 (2009).
86. Zhao, Y., Nielsen, C. P., Lei, Y., McElroy, M. B. & Hao, J. Quantifying the uncertainties of a bottom-up emission inventory of anthropogenic atmospheric pollutants in China. *Atmos. Chem. Phys.* **11**, 2295–2308 (2011).
87. Liu, Z. et al. Reduced carbon emission estimates from fossil fuel combustion and cement production in China. *Nature* **524**, 335–338 (2015).
88. Li, M. et al. Anthropogenic emission inventories in China: a review. *Natl. Sci. Rev.* **4**, 834–866 (2017).
89. Bond, T. C. et al. Bounding the role of black carbon in the climate system: A scientific assessment. *J. Geophys. Res. Atmos.* **118**, 5380–5552 (2013).
90. Cucurachi, S., Sala, S., Laurent, A. & Heijungs, R. Building and characterizing regional and global emission inventories of toxic pollutants. *Environ. Sci. Technol.* **48**, 5674–5682 (2014).
91. Tibrewal, K. et al. Assessment of methane emissions from oil, gas and coal sectors across inventories and atmospheric inversions. *Commun. Earth Environ.* **5** <https://doi.org/10.1038/s43247-023-01190-w> (2024).
92. Qiu, X., Liu, M. & Wang, X. Supplementary data for “Declines in anthropogenic mercury emissions in the Global North and China offset by the Global South”. figshare. <https://doi.org/10.6084/m9.figshare.26539714.v3> (2025).

Acknowledgements

This study was funded by the National Natural Science Foundation of China (Grant Nos. 42476127 and 41821005) and supported by the High-Performance Computing Platform of Peking University. M.L. was also supported by the Fundamental Research Funds for the Central Universities (Grant No. 7100604309) and Laboratory for Earth Surface Processes, Ministry of Education, Peking University. Q.Z. also acknowledges the funding from the China Postdoctoral Science Foundation (2022M720005) and the Beijing Natural Science Foundation (Grant No. 8244068).

Author contributions

S.T., X.W., H.S., G.S., M.L., and X.Q. conceived the initial framework. X.Q., Yuanzheng Z., J.L., R.D., S.Z., J.W., Yaqi Z., H.S., and G.S. were involved in data collection and cleaning. X.Q., Yuanzheng Z., H.L., X.C., and Q.Z. performed the modelling and carried out the analysis. M.L. and X.W. supervised and coordinated the overall research. X.Q. and M.L. drafted the manuscript with all other authors contributing to the writing, revisions and editing.

Competing interests

The authors declare no competing interests.

Additional information

Supplementary information The online version contains supplementary material available at <https://doi.org/10.1038/s41467-025-56274-2>.

Correspondence and requests for materials should be addressed to Maodian Liu or Xuejun Wang.

Peer review information *Nature Communications* thanks Anne-Helene Fostier and the other, anonymous, reviewer(s) for their contribution to the peer review of this work. A peer review file is available.

Reprints and permissions information is available at <http://www.nature.com/reprints>

Publisher's note Springer Nature remains neutral with regard to jurisdictional claims in published maps and institutional affiliations.

Open Access This article is licensed under a Creative Commons Attribution-NonCommercial-NoDerivatives 4.0 International License, which permits any non-commercial use, sharing, distribution and reproduction in any medium or format, as long as you give appropriate credit to the original author(s) and the source, provide a link to the Creative Commons licence, and indicate if you modified the licensed material. You do not have permission under this licence to share adapted material derived from this article or parts of it. The images or other third party material in this article are included in the article's Creative Commons licence, unless indicated otherwise in a credit line to the material. If material is not included in the article's Creative Commons licence and your intended use is not permitted by statutory regulation or exceeds the permitted use, you will need to obtain permission directly from the copyright holder. To view a copy of this licence, visit <http://creativecommons.org/licenses/by-nc-nd/4.0/>.

© The Author(s) 2025